Low-Temperature Synthesis of Nano-to-Submicron Size Organo-Zinc Oxide and Its Effect on Properties of Polybutadiene Rubber

Madhuchhanda Maiti,[1] Avani Vaghasia,[2] Raksh Vir Jasra[1]

[1]*Reliance Technology Group, Vadodara Manufacturing Division, Reliance Industries Ltd., Vadodara 391346, Gujarat, India*
[2]*Department of Applied Chemistry, M. S. University, Vadodara 390002, Gujarat, India*

Received 3 December 2009; accepted 19 July 2011
DOI 10.1002/app.35306
Published online 3 November 2011 in Wiley Online Library (wileyonlinelibrary.com).

ABSTRACT: Nano-to-submicron sized particles of zinc oxide (ZnO) were synthesized by low temperature hydrolysis method. Organo-ZnO was also synthesized by the aforementioned method in presence of polyethylene glycol (PEG-2000). The synthesized ZnO particles were characterized by infra-red spectroscopy, X-ray diffraction, BET surface area, scanning electron microscopy (SEM), and transmission electron microscopy (TEM). FTIR showed that PEG was present on the ZnO surface. Organo-ZnO exhibited floral-shape morphology consisting of concentric nanorods. The average diameter of the nanorods was $\sim$ 250 nm as evident from SEM. TEM showed that the nanorods were made of $\sim$ 50 nm sized small particles. UV-absorbance property of ZnO was unaltered even after organic coating. Curing, physico-mechanical and thermal properties of polybutadiene rubber compounded with organo-ZnO were compared with those of standard commercial rubber grade ZnO and nano-ZnO prepared by high and low temperature methods. The cure-characteristics were studied with the help of moving die rheometer as well as differential scanning calorimetry (DSC). Crosslink-density measurement along the DSC vulcanization exotherm showed better cure efficiency of organo-ZnO. Organo-ZnO containing compound exhibited better mechanical and thermal properties.
 J Appl Polym Sci 124: 2857–2866, 2012

Key words: organo-ZnO; polybutadiene; curing of polymers; mechanical properties; thermal properties

INTRODUCTION

Zinc oxide (ZnO), an important chemical for the rubber industry, is commercially manufactured by the French and the American process.[1] In the French process pure metal is evaporated to obtain a pure oxide, whereas in the American process zinc vapor is obtained directly from a zinc ore by burning it with coal or electrothermally.[2] The conventional rubber grade ZnO has specific surface area in the range of 5–10 m^2/g.[2] ZnO has been proved as the most cost effective inorganic pigment to activate the rate of sulfur cure with the accelerators.

As it makes the vulcanizing reaction faster, ZnO is an essential additive that enables to reduce production cycle and thereby lowers the overall cost of the rubber products. Besides, it has other beneficial effects. For example, ZnO can protect rubber from the thermal effects caused by internal friction. ZnO acts as a "heat sink" which accepts frictional energy without a large increase in internal temperature.[3] Furthermore, its high thermal conductivity helps to dissipate local heat concentrations that could otherwise deteriorate the properties of the rubber.[4] ZnO not only improves the properties of vulcanized rubber but also assists the processing of uncured rubber. It can decrease the shrinkage of molded rubber products and can maintain the improved cleanliness of molds. This increases productivity by increasing the number of molding cycles that can be achieved between cleaning.

For better heat conductivity high loadings of ZnO are used in heavy-duty pneumatic tires, since heat-buildup is a critical problem at higher speed. But some adverse environmental effects of zinc exposure have been reported.[5,6] The main sources of zinc pollution are referred to be iron and steel production, nonferrous metals manufacture and road transport. The road transport emission is mainly due to tire wear. This arises from the zinc content (1 wt %) of the tire-tread material.[5,6] Therefore, ZnO nanoparticles which could do faster curing at reduced dosing could help in lowering the zinc emission.

ZnO nanoparticles have been studied as a cure activator and curing agent in natural rubber, styrene-butadiene rubber, nitrile-butadiene rubber, carboxylated nitrile-butadiene rubber, and chloroprene rubber.[7–10] However, to the best of our knowledge, the

Correspondence to: M. Maiti (madhuchhanda.maiti@ril.com).

effect of ZnO nanoparticles as cure activator has not yet been explored for polybutadiene rubber (BR).

There are different methods available in the literature to synthesize ZnO nanoparticles.[7–21] But most of the processes involve high temperature synthesis. There are also very few reports on organo-ZnO synthesis.[22,23] In this study, ZnO and organo-ZnO in the range of nano-to-submicron size were synthesized using low temperature method. The aim of this study is to synthesize ZnO and organo-ZnO nano-to-submicron size particles at low temperature and to investigate the effect of such ZnO as a cure activator and thermal stabilizer in polybutadiene rubber at lower loading level. The organo-ZnO was compared with the standard commercial rubber grade ZnO and ZnO nanoparticles prepared by precipitation and calcination method.

EXPERIMENTAL

Materials

Zinc acetate, dihydrate [$Zn(CH_3COO)_2$. $2H_2O$] (99% purity) was procured from Sigma-Aldrich Chemicals, India. Ammonium carbonate [$(NH_4)_2CO_3$] (99% purity) was obtained from Merck (I), India. Sodium hydroxide (NaOH) and ethanol were supplied by Labort Fine Chem, India and Bengal Chemicals and Pharmaceuticals, India, respectively. Polyethylene glycol of molecular weight 2000, PEG-2000, sulfur, stearic acid (98% purity), standard commercial rubber grade ZnO (SZ), and *N*-Cyclohexyl-2-benzothiazole sulfenamide (CBS) (98% purity) were supplied by Labort Fine Chem, India. BR (Cisamer 01) was obtained from Reliance Industries Ltd., India.

Synthetic routes used for preparation of ZnO nanoparticles are discussed below:

Method 1: Precipitation and calcination method

Zinc acetate, dihydrate and ammonium carbonate were separately dissolved in distilled water at concentration of 1.0*M*. Zinc acetate, dihydrate solution was then slowly dropped into the vigorously stirred ammonium carbonate solution with a molar ratio of 1 : 1.5 to prepare the ZnO precursor. A white precipitate formed immediately on mixing the two solutions, but it dissolved with stirring. The equilibrium state was slowly achieved because of the high concentration of Zn^{2+} ions. The solid was collected by filtration, repeatedly rinsed with ethanol, and then dried at 100°C for 12 h. ZnO particles were obtained after calcination at 400°C for 2 h. The product was designated as Z1.

Method 2: Low temperature method

A total of 0.5*M* Zinc acetate, dihydrate and 1 *M* NaOH solution in ethanol were reacted for 6 h at 70–75°C to have ZnO. The product was filtered and repeatedly rinsed with ethanol and dried at room temperature in a vacuum oven. The product was designated as Z2.

Method 3: Synthesis of Organo-ZnO

A total of 0.5*M* Zinc acetate, dihydrate and 1*M* NaOH solution in ethanol were taken. 1 g PEG-2000 was dissolved in 4 mL of ethanol and added to the above solution and then reacted for 6 h at 70–75°C to have organo-ZnO. The product was filtered and repeatedly rinsed with ethanol and dried at room temperature in a vacuum oven. The product was designated as Z3.

Characterization methods

Morphology

Morphology studies of different ZnO samples were performed by using scanning electron microscope (SEM) (JEOL JSM-5800, Japan) at 20 kV of acceleration voltage at room temperature. Samples were taken as prepared and sputter coated with thin gold layer before scanning.

Morphology of different ZnO samples was also investigated by transmission electron microscopy (TEM) (JEOL 2010). The samples were dispersed in acetone by ultrasonication and then a drop of it was deposited on carbon coated copper grid and was analyzed under an accelerating voltage of 200 KV.

X-ray diffraction (XRD)

X-ray diffraction analysis was done using X-ray diffractometer (Rigaku CN2005, "Miniflex" model) in the range 10–75° (= 2θ). The zinc oxide powder was deposited on the sample holder uniformly.

Fourier transform infra-red spectroscopy (FTIR)

FTIR analysis was done using Nicolet 6700, in the range of 400–4000 cm^{-1} by making KBr pellet of the samples. 5 mg of sample was used to make the pellets.

UV spectroscopy

UV spectra were measured in the range of 200–800 nm using Perkin–Elmer UV/vis/NIR (Lambda 19) spectrometer in diffuse reflectance spectroscopy (DRS) mode.

BET surface area measurement

BET surface area measurement was done using Micromeritics (ASAP-2020) instrument. The samples were activated at 200°C for 6 h under vacuum (10 mmHg)

TABLE I
Formulations and Designation of Different BR Compounds

Compound designation	BR-SZ	BR-Z1	BR-Z2	BR-Z3
Formulation, phr[a]	BR-100	BR-100	BR-100	BR-100
	ZnO-3	ZnO-3	ZnO-3	ZnO-3
	CBS-0.8	CBS-0.8	CBS-0.8	CBS-0.8
	Sulfur-2	Sulfur-2	Sulfur-2	Sulfur-2
	Stearic acid-1.5	Stearic acid-1.5	Stearic acid-1.5	Stearic acid-1.5
ZnO used	SZ	Z1	Z2	Z3

[a] phr = parts per hundred gram of rubber.

before measurements. Five point BET surface area and total pore volume are measured. The average of five readings is reported along with the standard deviation.

Preparation and characterization of rubber composites

Compounding and vulcanization

ZnO was mixed with rubber by melt mixing method using Brabender Plasticorder (Germany) at 100°C and 60 rpm rotor speed. The formulations and designation are described in Table I. Amount of ZnO used was lower than that used in the conventional formulations.

The sample was then passed through a laboratory two-roll open mixing mill at a friction ratio 1 : 1.2. The rolls were cooled to room temperature by continuous circulation of water. The curing studies were followed with a Moving Die Rheometer (Monsanto model, MDR 2000) at 145°C temperature. Samples were cured at optimum cure time in a compression-molding machine (Moore press, Birmingham, UK) under 5 MPa pressure.

Differential scanning calorimetry (DSC)

Cure-studies were done using differential scanning calorimetric analysis. It was carried out using modulated DSC (DSC 2910, TA Instruments). The samples were heated from ambient temperature to 250°C (at 5°C/min heating rate) in air. A total of 5 mg of each sample was taken for the measurement. The error limit in the "weighing measurements" was within ± 5%.

Physicomechanical properties

Tensile and tear properties

Tensile test of the samples was carried out according to ASTM D 412-98a on dumb-bell shaped specimens using a Hounsfield H25KS universal testing machine at ambient temperature at a crosshead speed of 500 mm/min and tear samples were measured by using a Hounsfield H25KS universal testing machine according to ASTM D 624-00.

Hardness

Hardness of each composition was obtained using Shore A Durometer tester as per ASTM D 2240-97.

Thermogravimetric analysis (TGA)

Thermogravimetric analysis was done using thermogravimetric analyzer (model Hi-Res TGA 2950, TA Instruments). The samples were heated from ambient temperature to 700°C (at 10°C/min heating rate) in the furnace of the instrument under dynamic nitrogen atmosphere flowing at 60 mL/min. A total of 10 mg of each sample was taken for the measurement.

Swelling studies

The cured samples were immersed in toluene for 72 h at 25°C temperature. The volume fraction of rubber in the swollen gel, at equilibrium swelling, was calculated using eq. (1):

$$V_r = \frac{(D - FT)\rho_r^{-1}}{(D - FT)\rho_r^{-1} + A_0\rho_s^{-1}} \quad (1)$$

where, D = Deswollen Weight

F = Weight fraction of the insoluble component

T = Initial weight of the test specimen

ρ_r = Density of rubber

ρ_s = Density of solvent

A_0 = Amount of solvent absorbed

Further, the crosslink density, $\frac{1}{2M_c}$, in mol/g of rubber hydrocarbon was calculated using the Flory-Rehner eq. (2):

$$-[\ln(1 - V_r) + V_r + \chi V_r^2] = \frac{\rho_r V(V_r^{1/3} - V_r/2)}{2M_c} \quad (2)$$

χ = Flory Huggins interaction parameter, 0.46 for BR-toluene system[24]

V = Molar volume of swelling solvent

M_C = Number average molecular weight of the chain between two crosslinks.

RESULTS AND DISCUSSION

Zinc oxide nanoparticles were prepared from the solution of zinc acetate by high temperature calcination method as well as low temperature hydrolysis methods. The prepared ZnO particles were characterized by FTIR, XRD, UV, SEM, and TEM, which has been discussed in the following sections.

FTIR

FTIR spectra of different ZnO samples are depicted in Figure 1(a–f). Figure 1(a) shows the FTIR of dried precursor obtained in method 1. In the FTIR spectrum, the characteristic O—H stretching band centered at 3342 cm^{-1} is observed in addition to the v_3 mode of carbonate at 1527 and 1412 cm^{-1}.[25] The precursor is considered to be a basic salt of zinc carbonate ($ZnCO_3$) having a formula like $Zn_5(CO_3)_2(OH)_6$.[26]

It was calcined at 250°C for 6 h. The FTIR spectrum of the product is shown in Figure 1(b). There is a peak at $\sim$ 432 cm^{-1}, which is a characteristic of ZnO,[15,27] as seen in the FTIR spectrum of standard commercial rubber grade ZnO (SZ) [Fig. 1(c)]. This band corresponds to Zn-O stretching. In Figure 1(b), there are some peaks at 1588, 1421, and 1340 cm^{-1} which corroborate to the presence of basic $ZnCO_3$ intermediates as aforementioned. To confirm it, dil. HCl was added to this sample and bubbling was observed immediately. It proves that calcination at 250°C for 6 h is not sufficient for complete conversion of the precursor to ZnO.

The precursor was then calcined at 400°C for 2 h to have the sample Z1. The FTIR spectrum of Z1 is shown in Figure 1(d). Peaks of intermediate were absent in sample Z1. It was further confirmed with dil. HCl test. There was no bubbling after addition of dil. HCl in Z1. The peak of ZnO can be seen at 432 cm^{-1} which matches well with SZ. Hence, calcination at 400°C for 2 h can lead to complete conversion of basic $ZnCO_3$ to ZnO.

The precursor was formed according to the following eq. (3):

$$5Zn(CH_3COO)_2 + 5(NH_4)_2CO_3 + 3H_2O \rightarrow \underset{(\text{Precursor})}{Zn_5(CO_3)_2(OH)_6} + 10NH_4(CH_3COO) + 3CO_2 \quad (3)$$

The thermal decomposition of the precursor is expressed by the following chemical eq. (4):

$$Zn_5(CO_3)_2(OH)_6 \rightarrow 5ZnO + 2CO_2 + 3H_2O \quad (4)$$

The precursor was subjected to TGA analysis. The TGA curve is shown in Figure 1(g). The basic zinc carbonate decomposes at around 220°C. The residue (74%) correspondence to the amount of ZnO as theoretically calculated from eq. (4). Hence, the precursor decomposes in the way as predicted in eq. (4).[28,29]

In method 2, $Zn(CH_3COO)_2.2H_2O$ was hydrolyzed with alcoholic NaOH at low temperature (70°C) to have the sample Z2. The FTIR spectrum of the product is shown in Figure 1(e). It shows a peak at 432 cm^{-1} for ZnO.

Figure 1(f) illustrates the spectrum of ZnO prepared by hydrolysis of $Zn(CH_3COO)_2.2H_2O$ at 70°C in presence of PEG-2000. The FTIR spectrum of Z3 shows peak for ZnO at 432 cm^{-1} along with characteristic peaks of PEG at around 2927 and 2851 cm^{-1} for C—H stretching vibrations, 1500 and 1386 cm^{-1} for C-H deformations, 1109 cm^{-1} for C—O ether stretching and at around 3433 cm^{-1} for alcoholic O-H stretching vibration.[27] It indicates that these ZnO particles are wetted with PEG, i.e., PEG molecules are still present on the surface of ZnO particles.

XRD

Figure 2 presents the X-ray diffraction patterns of different of synthesized ZnO samples. All of the indexed peaks in the obtained diffractograms match with that of the bulk ZnO [JCPDS card # 79-0207], which confirm that the synthesized samples are of wurtzite hexagonal structure.[16] Any peak related to impurities was not detected in the diffractogram within the detection limit of the XRD. Starting material, $[Zn(CH_3COO)_2.2H_2O]$, shows small peaks at 27, 38, 42, and 44°.[15] Absence of these peaks in the diffractograms of final products indicates the purity of the products. The *d*-spacing values of the peaks of the final products also coincide with the bulk ZnO.

The average crystallite size was determined by Scherrer eq. (5):[30]

$$L = \frac{K\lambda}{\beta\cos\theta} \quad (5)$$

where, β is the full-width at half maximum, K is a constant approximately equal to unity, λ is the incident wavelength of CuK_α radiation ($\lambda = 0.154$ nm), L is the crystallite size, and θ is the diffraction angle at a certain crystal plane.

The average crystallite size of Z1, Z2, and Z3, calculated using eq. (5) with the (100) peak, is found to be 26, 28, and 23 nm. It shows that the average crystallite size of organo-ZnO is the smallest. It should be noted that crystallite size is assumed to be the size of a coherently diffracting domain. It is not necessarily the same as particle size.[30]

BET surface area measurements

Surface area and pore volume both increase by manifold in the synthesized ZnO samples compared

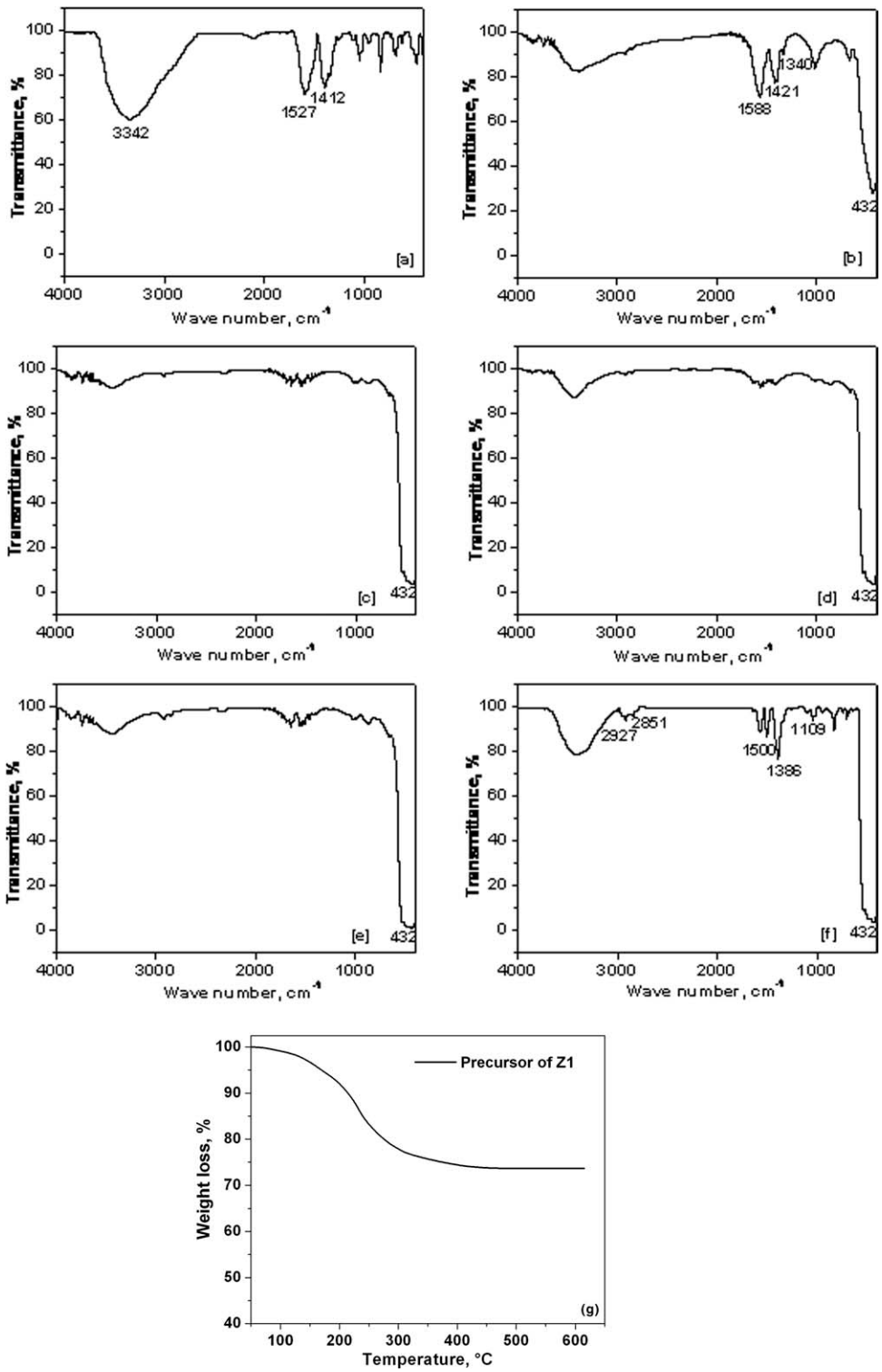

Figure 1 FTIR spectra of (a) precursor of method 1, (b) precursor of method 1 calcined at 250°C for 6h, (c) SZ, (d) Z1, (e) Z2 and (f) Z3. (g) TGA plot of precursor of Z1.

with that of SZ (Table II). The surface area increases in the order of Z1 < Z2 < Z3. The better polymer-filler interaction can be expected from increased surface area of the synthesized ZnO. Moreover, higher surface area indicates lower particle size in organo-ZnO.

UV absorbance

ZnO is known for its excellent UV absorption in the range of 290–390 nm (Figure 3). No absorbance peak can be observed in the spectrum for the precursor of Z1, basic zinc carbonate (Figure 3). The spectrum of

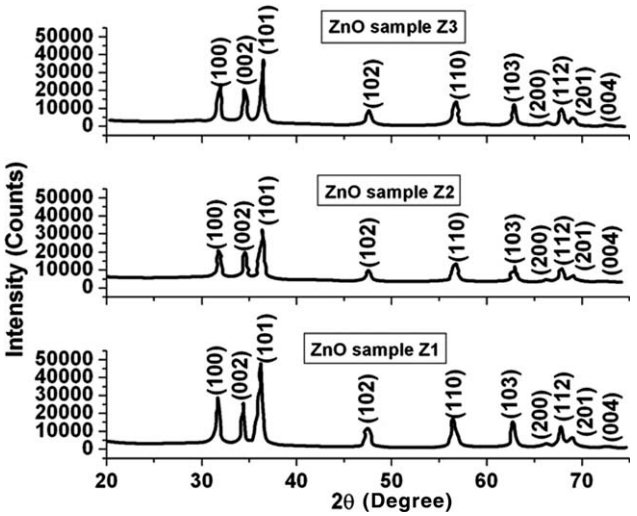

Figure 2 XRD of different ZnO samples.

Z1 shows strong absorbance in the range of 290–390 nm, which further supports the formation of ZnO particles. The spectrum of Z3 also exhibits absorbance peak in the range of 290–390 nm (Fig. 3). It indicates that organic coating does not hamper the UV absorbance properties of synthesized ZnO particles.

SEM

Morphology of different synthesized ZnO particles is studied by SEM. SEM image of Z1, the ZnO synthesized by method 1, shows aggregation of micron size particles of undefined morphology [Fig. 4(a)]. The sample has broader particle size distribution compared with Z2 [Fig. 4(b)].

SEM micrograph of sample Z2, prepared at low temperature, exhibits microstructural homogeneities through the entire area of the sample, indicative of a continuous, ZnO nanostructure network consisting of uniformly distributed sub-micropores on the surface as shown in Figure 4(b). It has a narrow particle size distribution.

A totally different morphology can be observed in the case of Z3 [Fig. 4(c)]. The rod-like particles are clubbed together at a common center giving a floral shape. The average rod diameter is $\sim$ 250 nm. These nano-rods have an average length of 1 μm. These concentric nanorods are generated from a center giving rise to floral shape. The growth process of the floral shaped ZnO nanostructure can be explained by the nature of PEG-2000. PEG is a nonionic surface active agent. The O-atom, of PEG is the hydrophilic group and the $-CH_2-CH_2-$ is the organophilic group. So, it is a long chain molecule containing both hydrophilic and organophilic groups.

When $Zn(CH_3COO)_2.2H_2O$ and NaOH were mixed, the reaction precursors were formed from Zn^{2+} and OH^- ions. The overall reactions are shown below:

$$Zn(CH_3COO)_2.2H_2O + NaOH \rightarrow Zn(OH)_2 + 2CH_3COONa + 2H_2O \quad (6)$$

$$Zn(OH)_2 + 2H_2O \rightarrow \underset{\text{(Precursor)}}{[Zn(OH)_4]^{2-}} + 2H^+ \quad (7)$$

This precursor is extremely unstable; when heated at 70°C, it will decompose to form ZnO, according to eq. (8).

$$[Zn(OH)_4]^{2-} \rightarrow ZnO + H_2O + 2OH^- \quad (8)$$

The Zn^{2+} ions can act on the hydrophilic portion of PEG chains. Thus, the reaction precursor will grow at the hydrophilic portion of PEG-2000; the precursor will decompose to form ZnO and thus the ZnO particles will grow along PEG-2000, leading to a floral shaped organo-ZnO.[31–33]

TEM of synthesized ZnO

TEM of synthesized ZnO has been illustrated in Figure 5(a,b). Figure 5(a) shows the TEM image of Z2. It shows that particles of $\sim$ 50 nm are aggregated together to give a bigger cluster of $\sim$ 250 nm. Figure 5(b) is the TEM image of Z3. The figure

TABLE II
BET Surface Area of Different ZnO Samples

Sample	Surface area (m^2/g)	Pore volume (cm^3/g)
SZ	05 ± 0.03[a]	0.033
Z1	18 ± 0.10	0.124
Z2	37 ± 0.18	0.157
Z3	41 ± 0.29	0.214

[a] Standard deviation.

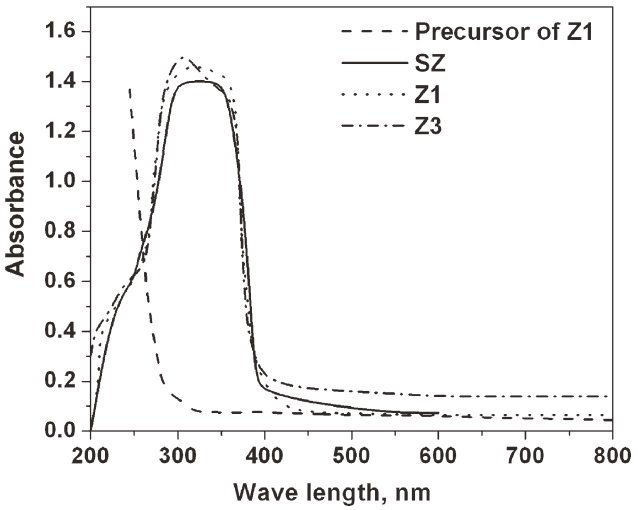

Figure 3 UV absorbance of different ZnO samples.

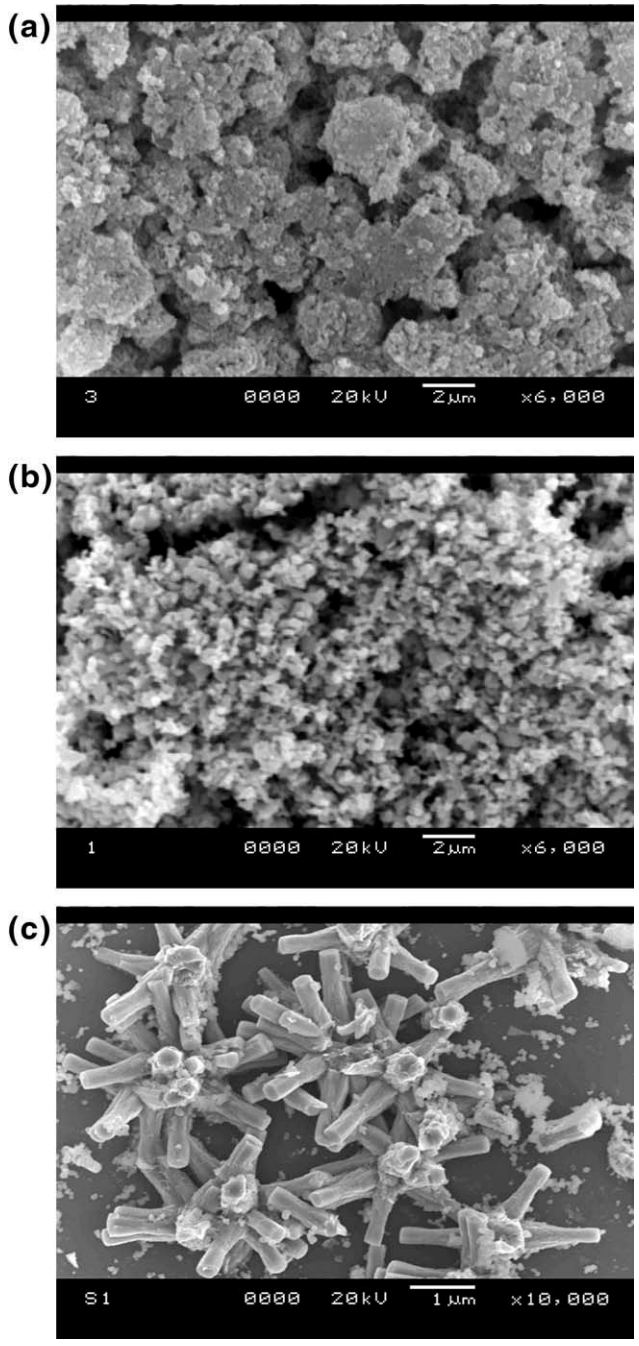

Figure 4 SEM image of ZnO sample (a) Z1, (b) Z2 and (c) Z3.

exhibits small particles of ~ 50 nm forming a 1 µm long rod-like structure. The exact floral-shape could not be observed in TEM. This may be due to dispersion of nanorods under the influence of ultrasonic vibration during sample preparation for TEM.

Effect of synthesized ZnO on curing properties of BR

The rheographic profile of different compounds, BR-SZ, BR-Z1, BR-Z2, and BR-Z3 at 145°C is represented

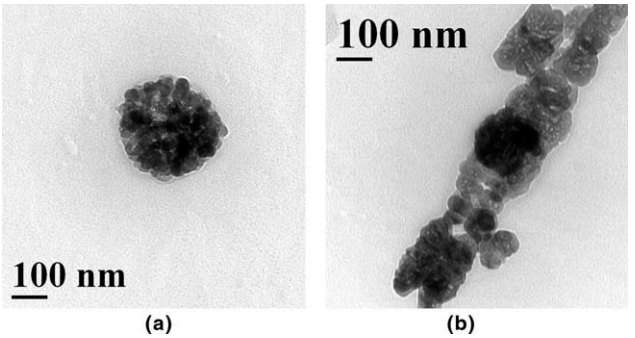

Figure 5 (a) TEM image of ZnO sample Z2. (b) TEM image of ZnO sample Z3.

in Figure 6 and the cure characteristics are tabulated in Table III. The difference in minimum and maximum torque value, $\Delta S = (M_H\text{-}M_L)$, is higher for BR-Z3 than BR-Z2, BR-Z1, and BR-SZ. Increased ΔS indicates resistance to polymer chain mobility.[34] Because of formation of more crosslinks, chain mobility is restricted here which will lead to higher crosslink density as discussed later.

"Cure time" is measured as the time in minutes to reach 90% of maximum torque.[35] The curing is faster with synthesized ZnO samples compared with the commercial one. The maximum torque of synthesized ZnO samples is also slightly higher than that of standard one. ZnO helps in producing the vulcanization precursor after reacting with accelerator as reported in literature and acts as a cure activator.[36,37] Because of the smaller particle size of synthesized ZnO, the area of contact increases which helps to react better with accelerator. This leads to the generation of vulcanization precursor quicker. It results in a faster curing rate and lower cure time. It can be also observed that cure-time decreases with increasing surface area of the synthesized ZnO particles. It also supports the above explanation. The curing is fastest with the organo-ZnO (Z3), which also has

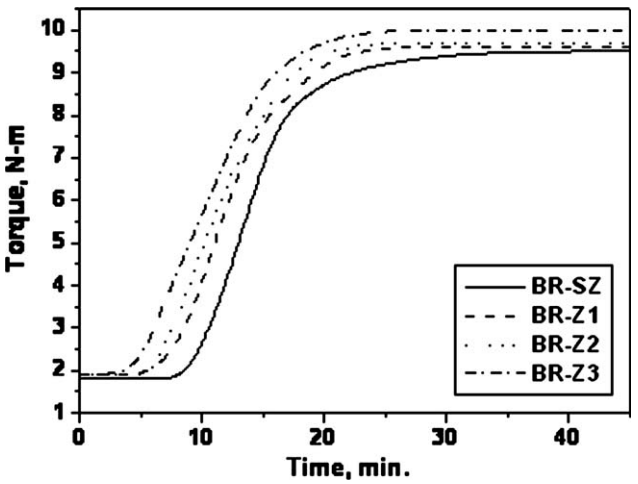

Figure 6 Cure curves for BR compounds.

TABLE III
Cure Characteristics of Different ZnO Based BR Compounds

Cure characteristics	BR-SZ	BR-Z1	BR-Z2	BR-Z3
Cure time (min)	19 ± 0.05[a]	18 ± 0.02	17 ± 0.03	15 ± 0.02
Maximum torque (N-m)	9.5 ± 0.01	9.6 ± 0.01	9.7 ± 0.02	10± 0.02
ΔS, (N-m)	7.7± 0.01	7.7± 0.01	7.8± 0.01	8.1± 0.02

[a] Standard deviation.

largest surface area. This may be due to the fact that organic coating makes the ZnO more compatible with butadiene rubber which coupled with highest surface area leads to better dispersion of the ZnO particles.

Crosslink density of rubber samples containing different ZnO

Effect of organo-ZnO as activator has been studied in details with the help of DSC in line with the work by Hendrikse et al. and Kruger and McGill.[38,39] The DSC curves obtained upon heating compounded BR with different ZnO at 5°C/min rate in air atmosphere, show a broad exotherm, with the onset at approximately 185°C (Fig. 7). The peak maximum is obtained at around 190°C for BR-Z3 while maxima are found at around 195°C for BR-SZ, BR-Z1 and BR-Z2. It indicates faster curing in BR-Z3 than the other two. Another exotherm can be observed (peak at around 230°C) due to further reactions of degradation. The reaction was stopped at points along the DSC curve and samples were swelled in toluene. Crosslink density values for different samples are shown as inset in Figure 7. The highest crosslink density (1.2×10^{-4} mol/g) is found in BR-Z3 compared with the other two samples. Crosslink density of BR-SZ, BR-Z1, and BR-Z2 is 7.1×10^{-5}, 7.6×10^{-5}, and 7.8×10^{-5} mol/g, respectively. The crosslink density passes through a peak. As crosslinking and degradation are two competitive processes, the lowering of crosslink density after achieving the maximum, indicates that chain breaking started predominating than crosslink formation. Subsequently,

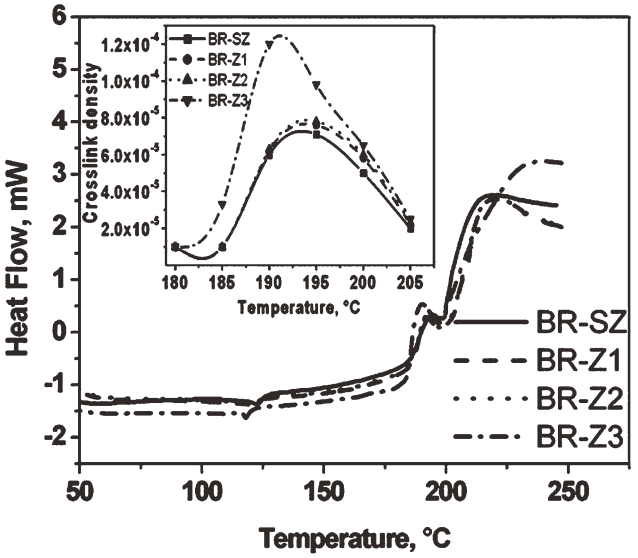

Figure 7 DSC curves of different ZnO containing BR compounds heated at 5°C/min; inset: corresponding crosslink density along the DSC exotherm.

another exotherm can be seen immediately after the crosslinking exotherm, which corresponds to the 1st step degradation of BR.[40]

Physico-mechanical properties of rubber compounds

The physico-mechanical properties of rubber compounds containing different ZnO samples are reported in Table IV. The sample containing organo-ZnO shows highest tensile strength as well as modulus at 100% elongation. This is due to better compatibility and in turn better dispersion of organo-ZnO in the rubber matrix. This leads to better curing as observed in the previous experiments and higher value of volume fraction of rubber (V_r). Besides, organo-ZnO has particle size in nano range. Hence, it can behave like nanofillers as well. Tensile strength of BR-Z3 is higher by 55, 33, and 35% than that of BR-SZ, BR-Z1, and BR-Z2, respectively. The better compatibility of organo-ZnO with the rubber matrix leads to enhanced properties even compared with Z2 (nanoparticles without organic coating). The floral shaped organo-ZnO is consisting of concentric

TABLE IV
Physico-Mechanical Properties of Different BR Compounds

Sample	Tensile strength (MPa)	Elongation at break (%)	Modulus at 100% elongation (MPa)	Tear strength, (N/mm)	Hardness (Shore A)	V_r
BR-SZ	1.00 ± 0.05[a]	170 ± 5	0.80 ± 0.02	5.46 ± 0.57	42	0.174 ± 0.007
BR-Z1	1.16 ± 0.04	205 ± 10	0.75 ± 0.01	6.18 ± 0.23	44	0.180 ± 0.001
BR-Z2	1.15 ± 0.04	200 ± 10	0.78 ± 0.02	6.20 ± 0.19	44	0.183 ± 0.002
BR-Z3	1.55 ± 0.05	175 ± 5	1.12 ± 0.04	6.79 ± 0.15	45	0.214 ± 0.005

[a] Standard deviation.

nanorods. These nanorods can prevent crack propagation which may be the reason for higher tear value in BR-Z3.

Thermal properties of the synthesized ZnO containing rubber compounds

Typical thermogravimetric (TG) curves and the corresponding derivative thermogravimetric (DTG) curves obtained at a heating rate of 10°C/min in nitrogen (N_2) atmosphere for BR, BR-SZ, BR-Z1, BR-Z2, and BR-Z3 are shown in Figure 8(a,b). Two-step degradation is observed in the case of neat BR. The 1st step is said to be almost exclusively due to volatile depolymerization products. The 2nd is attributed to degradation of a residue due to cyclized and crosslinked BR.[41] The TG curves exhibit two-step degradation in the case of synthesized nano-ZnO containing rubber composites. Hence, the degradation mechanism of BR remains unaltered in the presence of nano-ZnO particles. T_{max}, residue and maximum rate of decomposition values for the above-mentioned samples are reported in Table V. Each type of nano-ZnO imparts thermal stability to BR. A shift of T_{max} by around 12°C toward higher temperature can be observed in the case of the synthesized nano-ZnO containing samples compared with the standard one. There is a significant reduction in the rate of decomposition in the presence of the synthesized nano nano-ZnO at major degradation step. This may be due to the lower particle size and higher surface area of these nano-ZnO samples which can act as a better heat sink. The residue amount is same for BR-SZ, BR-Z1, and BR-Z2, but it is less for BR-Z3. As Z3 has some organic coating, it will have lesser amount of oxides at a particular loading. The organic portion will degrade with the polymer, so the net residue is less in this case.

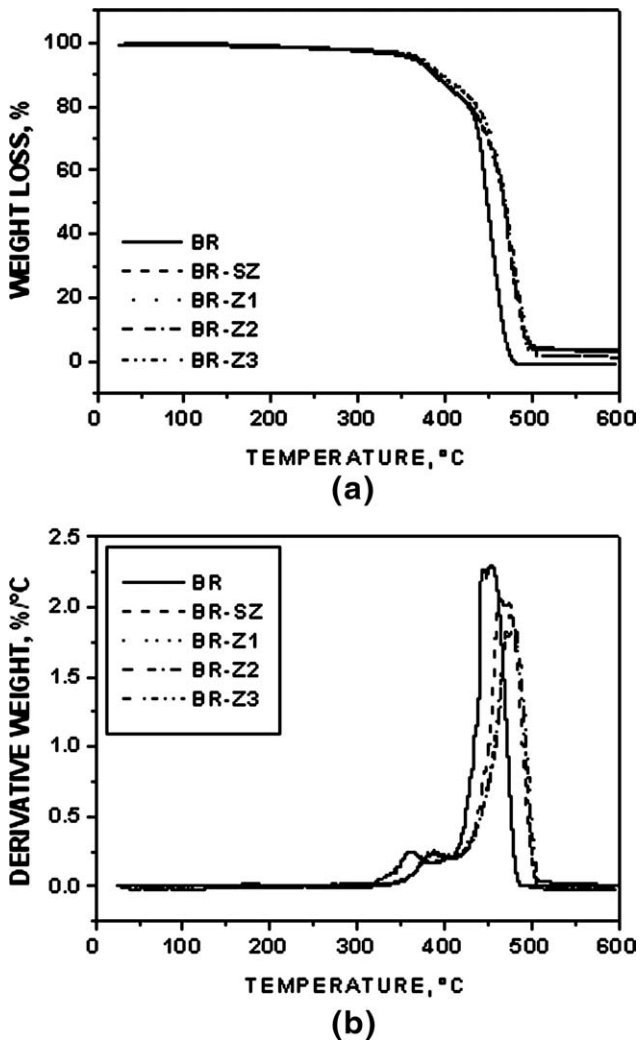

Figure 8 (a) TGA plots of different ZnO based BR compounds. (b) DTG plots of different ZnO based BR compounds.

TABLE V
Parameters Obtained from the Thermal Degradation of Different ZnO Based BR Compounds

Sample	T_{max} (°C)	Residue (%)	Maximum rate of decomposition (%/°C)
BR	452	0.0	2.31
BR-SZ	465	3.0	2.05
BR-Z1	477	3.0	1.95
BR-Z2	477	3.0	1.93
BR-Z3	478	1.9	1.82

CONCLUSIONS

ZnO and organo-ZnO of nano-to-submicron size particles were synthesized using low temperature hydrolysis method. The organo-ZnO shows a floral-shape morphology consisting of concentric rods of average diameter ~ 250 nm and 1 μm length. TEM shows that nanorods observed under SEM are made of small particles of 50 nm size. The organo-ZnO has a pronounced effect on curing. It causes a faster curing compared to the conventional commercial ZnO. It also improves physico-mechanical properties and imparts better thermal stability to the butadiene rubber compound due to better compatibility with the rubber matrix in presence of organic coating.

The Authors are thankful to Prof. J. Dave, Dr. Jince Sebastian, Dr. Pradip Munshi, and Mr. Suraj K. Kusum for their support.

References

1. Morton, M. Introduction to Rubber Technology; Reinhold Publishing Corporation: New York, 1959.
2. Wypych, G. Handbook of Fillers; William Andrew, Inc.: New York, 1999.
3. Depew, H. A. Ind Eng Chem 1933, 25, 532.
4. Barnett, C. E.; Mathews, W. C. Ind Eng Chem 1934, 26, 1292.

5. Councell, T. B.; Duckenfield, K. U.; Landa, E. R.; Callender, E. Environ Sci Technol 2004, 38, 4206.
6. Smolders, E.; Degryse, F. Environ Sci Technol 2002, 36, 3706.
7. Sahoo, S.; Maiti, M.; Ganguly, A.; George, J. J.; Bhowmick, A. K. J Appl Polym Sci 2007, 105, 2407.
8. Sahoo, S.; Bhowmick, A. K. J Appl Polym Sci 2007, 106, 3077.
9. Jincheng, W.; Yuehui, C. J Appl Polym Sci 2006, 101, 922.
10. Kim, I.; Kim, W.; Lee, D.; Kim, W.; Bae, J. J Appl Polym Sci 2010, 117, 1535.
11. Bacsa, R. R.; Dexpert-Ghys, J.; Verelst, M.; Falqui, A.; Machado, B.; Bacsa, W. S.; Chen, P.; Zakeeruddin, S. M.; Graetzel, M.; Serp, P. Adv Funct Mater 2009, 19, 875.
12. Bigdeli, F.; Morsali, A.; Retailleau, P. Polyhedron 2010, 29, 801.
13. Bhat, D. K. Nanoscale Res Lett 2008, 3, 31.
14. Zhang, J.; Sun, L.; Yin, J.; Su, H.; Liao, C.; Yan, C. Chem Mater 2002, 14, 4172.
15. Sivakumar, M.; Towata, A.; Yasui, K.; Tuziuti, T.; Iida, Y. Chem Lett 2006, 35, 60.
16. Bhattacharyya, S.; Gedanken, A. Micropor Mesopor Mat 2008, 110, 553.
17. Long, T.; Yin, S.; Takabatake, K.; Zhnag, P.; Sato, T. Nanoscale Res Lett 2009, 4, 247.
18. Cho, S.; Kim, S.; Kim, H.-J.; Lee, B. R.; Lee, K-H. Langmuir 2009, 25, 10223.
19. Carnes, C. L.; Klabunde K. J. Langmuir 2000, 16, 3764.
20. Suchanek, W. L. J Cryst Growth 2009, 312, 100.
21. Wu, P.; Pike, J.; Zhang, F.; Chan, S. Int J Appl Ceram Tec 2006, 3, 272.
22. Xiong, H.-M.; Wang, Z.-D.; Liu, D.-P.; Chen, J.-S.; Wang, Y-G.; Xia, Y-Y. Adv Funct Mater 2005, 15, 1751.
23. Anžlovar, A.; Orel, Z. C.; Žigon, M. Eur Polym Mater 2010, 46, 1216.
24. Gundert, F.; Wolf, B. A. In Polymer Handbook, 3rd ed.; Brandrup, J., Immergut, E. M., Eds.; John Wiley and Sons, Inc, New York, 1989.
25. Stoilova, D.; Koleva, V.; Vassileva, V. Spectrochim Acta Part A 2051, 2002, 58.
26. Koga, N.; Matsuda, Y.; Tanaka, H. Chem Educator 2005, 10, 440.
27. Alojz, A.; Crnjak, Z.; Zigon, O. M. Polimeri 2008, 29, 84.
28. Zhang, S.; Fortier, H.; Dahn, J. R. Mater Res Bull 1939, 2004, 39.
29. Kanari, N.; Mishra, D.; Gaballah, I.; Dupré, B. Thermochimica Acta 2004, 410, 93.
30. Klug, H. P.; Alexandar, L. E. X-Ray Diffraction Procedures for Polycrystalline and Amorphous Materials; Wiley: New York, 1962.
31. Wang, J.; Zhang, S.; You, J.; Yan, H.; Li, Z.; Jing, X.; Zhang, M. Bull Mater Sci 2008, 31, 597.
32. Zhang, H.; Yang, D.; Ji, Y.; Ma, X.; Xu, J.; Que, D. J Phys Chem B 2004, 108, 3955.
33. Wahab, R.; Ansari, S. G.; Kim, Y. S.; Khang, G.; Shin, H.-S Appl Surf Sci 2037, 2008, 254.
34. Shamugharaj, A. M.; Bae, J. H.; Lee, K. Y.; Noh, W. H.; Lee, S. H.; Rye, S. H. Comp Sci Tech 2007, 67, 1813.
35. Brown, R. Physical Testing of Rubber; Chapman and Hall: London, 1996.
36. Coran, A. Y. In Science and Technology of Rubber; Eirich, F. R., Ed.; Academic Press: New York, 1978; Chapter 7.
37. Heideman, G.; Datta, R. N.; Noordermeer, J. W. M.; van Baarle, B. J Appl Polym Sci 2005, 95, 1388.
38. Hendrikse, K. G.; McGill, W. J.; Reedijk, J.; Nieuwenhuizen, P. J. J Appl Polym Sci 2000, 78, 2290.
39. Kruger, F. W. H.; McGill, W. J. J Appl Polym Sci 1992, 44, 581.
40. Brazier, D. W.; Schwartz, N. V. J Appl Polym Sci 1978, 22, 113.
41. Turi, E. A. Thermal Characterization of Polymeric Materials; Academic Press: New York, 1981.